TITAN: Thunderstorm Identification, Tracking, Analysis, and Nowcasting—A Radar-based Methodology

MICHAEL DIXON AND GERRY WIENER

Research Applications Program, National Center for Atmospheric Research, Boulder, Colorado

(Manuscript received 18 May 1992, in final form 25 January 1993)

ABSTRACT

A methodology is presented for the real-time automated identification, tracking, and short-term forecasting of thunderstorms based on volume-scan weather radar data. The emphasis is on the concepts upon which the methodology is based. A "storm" is defined as a contiguous region exceeding thresholds for reflectivity and size. Storms defined in this way are identified at discrete time intervals. An optimization scheme is employed to match the storms at one time with those at the following time, with some geometric logic to deal with mergers and splits. The short-term forecast of both position and size is based on a weighted linear fit to the storm track history data. The performance of the detection and forecast were evaluated for the summer 1991 season, and the results are presented.

1. Introduction

In convective situations, the forecasting problem encompasses storm initiation, evolution, and movement. For storm initiation, progress has been made in the use of data from sensitive Doppler radars to detect those boundary-layer features that are important for the forecast (Wilson and Schreiber 1986). Meanwhile, forecasters have identified the need for an objective procedure for detecting existing storms and extrapolating their evolution and movement (Wilson and Mueller 1993). This paper deals with the development of such a procedure.

Many of the techniques developed for the short-term forecasting of convective activity have incorporated some form of tracking, such as the extrapolation of the movement of features in the data. Pattern recognition (Austin 1985) uses the similarity of patterns in the data fields at successive times to deduce movement. The cross-correlation technique (Rinehart and Garvey 1978; Tuttle and Foote 1990) partitions the data fields into blocks or features, and identifies the movement vector that maximizes the correlation between a feature in the latest data field and the corresponding, but translated, feature in the previous data field. Both the pattern recognition and cross-correlation techniques treat the data as a *two-dimensional field* from which the movement of features may be inferred.

An alternative approach is to consider storms to be distinct *three-dimensional entities* that may be identified and for which physically based properties may be computed. These entities are then tracked by matching the storms at one time to their counterparts at a later time. This is referred to as "centroid tracking" (Austin and Bellon 1982). The advantage of this approach is that it makes more complete use of the information available; therefore, if done correctly, centroid tracking should produce better forecasts than the techniques based on two-dimensional data. In addition, this method provides a tool for the scientific analysis of storms as three-dimensional entities.

Crane (1979) presents a method in which two-dimensional cells are identified as regions around local maxima in the reflectivity field for a given PPI (plan position indicator). These cells are grouped into "volume cells" through the vertical association of cells in successive PPIs. The volume cells are tracked by estimating their velocity from past and present centroid locations, using this velocity to forecast the new position, and searching for cells close to the forecast position. For a recently formed storm, the steering-level wind is used as the forecast velocity. Witt and Johnson (1993) and Rosenfeld (1987) detail similar methods. In Witt's method, cells are defined as regions with reflectivity exceeding a given threshold, and the forecast velocity is based on a linear fit to the recent centroid history of the storm. The starting storm velocity is an operator-input value, which presumably would be set to the best guess for storm movement. Rosenfeld's method uses a reflectivity threshold to delineate a storm, and then identifies cells within the storm as regions around local maxima. The tracking technique is similar to Crane's but is more complicated and includes a check for overlap between the actual cell positions and their corresponding forecast locations.

Corresponding author address: Dr. Michael J. Dixon, Research Applications Program, NCAR, RAP/FW, P.O. Box 3000, Boulder, CO 80307-3000.

The method presented here is similar, in some respects, to those referred to above, in that storms are defined as three-dimensional regions of reflectivity exceeding a threshold and are logically matched from one scan time to the next. However, the identification method is much simpler and is based on radar data remapped into Cartesian coordinates, whereas the methods just referred to use data in radar coordinates with the associated geometrical complexity. The tracking component is based on an optimal solution to the matching problem, and no assumption is made about initial storm movement. Mergers and splits are identified through geometric logic about the storm positions and shapes. Forecasts are based on a weighted linear fit to the history of both the position and size of the storm. Throughout, the emphasis is on simplicity because many similar methods have a tendency to become overcomplicated.

The system is designed to keep pace with real-time radar data and to provide analysis and forecast results within 10 s or so of the end of a volume scan. The storm and track data are maintained in a database that permits analysis of the storm and track properties. The capability to display these properties during real-time data operations has been demonstrated. In addition, the track data are available for postanalysis of storm properties and the accuracy of the forecasts.

This methodology was originally developed, albeit in a somewhat simpler form, for the objective evaluation of a rain-augmentation experiment (Dixon and Mather 1986). Since mid-1990, the technique has been refined and enhanced as part of an effort to improve and automate convective nowcasting in the Denver region of Colorado.

2. Storm identification

a. *Storm definition*

The experimental unit is defined here as a contiguous region, all of which exhibits reflectivities above a given threshold (T_z), and the volume of which exceeds a threshold (T_v).

Clearly, the value of T_z determines the type of storm that will be identified. Some possibilities are

- individual convective cells, T_z = 40–50 dBZ,
- convective storms, T_z = 30–40 dBZ,
- mesoscale convective complexes, T_z = 25–30 dBZ,
- snow bands, T_z = 15–25 dBZ.

For this study, the experimental unit is the convective storm. To investigate the sensitivity of the method to the reflectivity threshold, T_z was set to 30, 35, and 40 dBZ. For all three cases the identification and tracking technique worked well. Obviously, the 40-dBZ storms were smaller and more intense (on average) than the 30-dBZ storms, and the lower the threshold the greater the number of apparent mergers.

Based on the results of the initial experiments, T_z was set to 35 dBZ for the final phase of the study. It should be borne in mind that the subject of this paper is the methodology, and that 35 dBZ was chosen as a threshold suitable for developing and evaluating the method. We are not suggesting that this is the correct or only threshold for studying convective storms. (Incidentally, the system was tested on snow band storms, at thresholds ranging from 15 to 25 dBZ, with promising results.)

The use of the volume threshold T_v is necessary to prevent the tracking of noise or small regions of residual ground clutter, and to keep the number of identified storms within reasonable limits. For this study, T_v was set to 50 km^3.

b. *Data preparation*

The storm identification technique may be applied to data in the radar coordinate system of range, azimuth, and elevation. In fact, the methodology was originally developed on radar-space data (Dixon and Mather 1986).

The geometry of a Cartesian coordinate system is much simpler, however, and this both aids one's conceptual understanding of the procedure and simplifies the computations of storm properties. Therefore, the radar coordinate data are transformed into Cartesian coordinates, and noise and ground clutter are filtered out. The details of these operations are given in appendixes A and B.

c. *The identification method*

To identify "storms" according to the definition given in section 2a, we need to find contiguous regions that have reflectivities above T_z. For clarity, this will be described in two dimensions (x, y). The concept is readily extended to incorporate the third (z) dimension.

Consider Fig. 1. Assume that all of the shaded squares represent Cartesian grid locations with reflectivity in excess of T_z. There are two steps to the procedure:

1) Identify contiguous sequences of points (referred to as runs) in one of the principal directions (in this case the x direction) for which the reflectivity exceeds T_z. There are 15 such runs in Fig. 1.

2) Group runs that are adjacent. A group of runs should contain all of the points in one storm. In this example, storm 1 comprises runs 1–6; storm 2 comprises runs 7, 8, and 10; storm 3 comprises runs 9, 11, 13, and 14; storm 4 contains only run 12; and storm 5, only run 15. Note that runs 5 and 7 are not considered adjacent since they only touch along a diagonal. The same applies to runs 12 and 15. It is likely that storms 4 and 5 would be rejected because they are

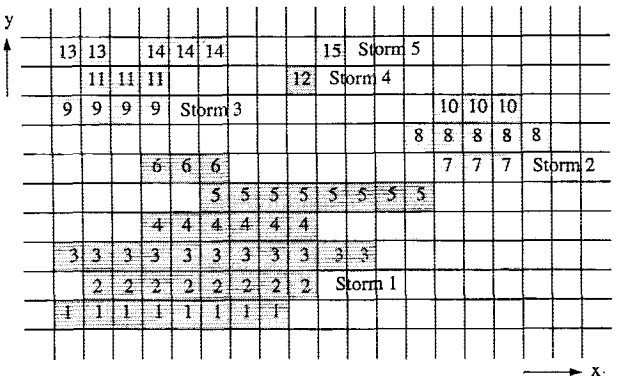

FIG. 1. Example of storm data runs—2D case. Shading indicates grid points where the reflectivity exceeds T_z. Different shades indicate different storms.

small. In the three-dimensional case, step 2 searches for adjacent runs in both y (alongside) and z (above or below).

The advantage of this two-step approach is that it reduces the dimensionality of the problem, making it more efficient computationally. In the case of a three-dimensional grid, once the runs have been found, the identification procedure reduces to a two-dimensional problem.

d. Storm analysis

For the purposes of the nowcasting experiment and storm analysis, a large number of storm properties were computed. These are listed in appendix C. However, only the following storm properties are relevant to this methodology:

- reflectivity-weighted centroid $(\bar{x}_z, \bar{y}_z, \bar{z}_z)$, using Z to weight the centroid computations,
- volume V,
- the size and shape of the area of the storm projected onto a horizontal plane (i.e., the area as it would appear from directly above the storm). The shape is approximated by an ellipse, which best fits the projected area as suggested by Zittel (1976) (Fig. 2). The ellipse properties are the centroid $(\bar{x}_e, \bar{y}_e)$, the major and minor radii $(r_{\text{major}}, r_{\text{minor}})$, and the orientation of the major axis relative to the x axis (θ).

The computation of the reflectivity-weighted centroid and volume is straightforward. The computation of the ellipse properties is based on a principal component transformation of the (x, y) data in the projected area. This is a rotational transform that yields axes along the principal components of the data (Richards 1986). In the two-dimensional case, these are the major and minor axes, which is why the transform is appropriate for the ellipse computations. The details are given in appendix E.

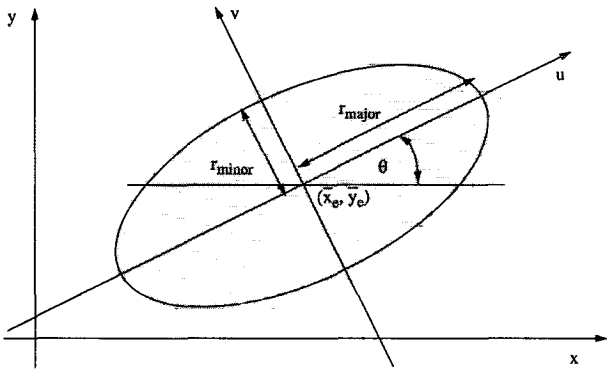

FIG. 2. Computation of projected-area ellipse parameters.

3. Tracking

a. Matching storm sets using combinatorial optimization

Figure 3 depicts the centroids and projected areas of two sets of storms, one set at time t_1 and the other at time t_2, the difference Δt being the time taken to collect a single volume scan (~5–10 min). There are not necessarily the same number of storms present at each time—in this example, there are 4 storms at t_1 and 5 storms at t_2. The figure also shows the possible paths the storms may have taken during the period between t_1 and t_2.

The problem is to match the t_1 storms with their t_2 counterparts, or equivalently to decide which set of logically possible paths most likely is the true one. If this is done for successive time intervals, the storms may be tracked for their entire duration.

Considering the figure, one may make the following intuitive assumptions:

1) The correct set will include paths that are shorter rather than longer. This is true for thunderstorms that are observed frequently ($\Delta t \sim 5$ min) because the ratio

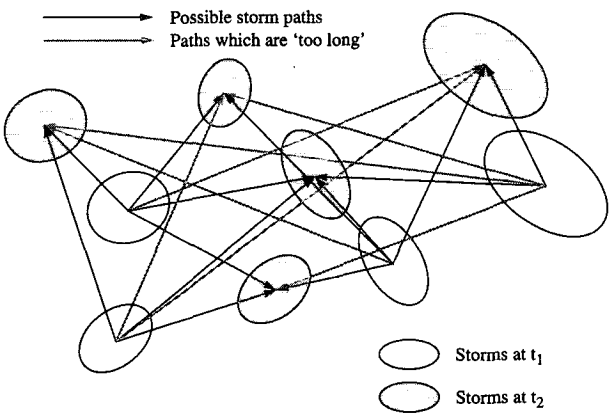

FIG. 3. Possible paths between storms at consecutive time intervals.

of the size of the storm (~3–10-km diameter) to the distance moved in Δt (~1–10 km) is such that it is unlikely that a storm will move well away, to have its former position (or one close to it) occupied by a different storm. Therefore, given a set of possible alternatives as shown in Fig. 3, the shorter the path the more likely it is to be a true one.

2) The correct set will join storms of similar characteristics (size, shape, etc.).

3) There is an upper bound to the distance a storm will move in Δt, governed by the maximum expected speed of storm movement (advection plus lateral development). In the figure, the paths that exceed this upper bound are drawn as faint lines.

The problem of determining the true set of storm paths may be posed and solved as one of optimization. We search for the optimal set of paths, where this set minimizes the cost function as defined below, and we assume that the optimal set and the true set are the same.

Suppose that a storm i at t_1 has state $\mathbf{S}_{1i} = (\bar{x}_{z1i}, \bar{y}_{z1i}, V_{1i})$, and storm j at t_2 has state $\mathbf{S}_{2j} = (\bar{x}_{z2j}, \bar{y}_{z2j}, V_{2j})$. Suppose too that there are n_1 storms at t_1 and n_2 storms at t_2.

We may define the "cost" C_{ij} (in units of distance) of changing state $\mathbf{S}_{1i}$ to state $\mathbf{S}_{2j}$ as

$$C_{ij} = w_1 d_p + w_2 d_v, \quad \text{where} \tag{1}$$

$$d_p = [(\bar{x}_{z1i} - \bar{x}_{z2j})^2 + (\bar{y}_{z1i} - \bar{y}_{z2j})^2]^{1/2} \quad \text{(assumption 1)}, \tag{2}$$

$$\text{and} \quad d_v = |V_{1i}^{1/3} - V_{2j}^{1/3}| \quad \text{(assumption 2)}. \tag{3}$$

Here d_p is a measure of the difference in position (i.e., the distance moved), d_v is a measure of the difference in volume (also in units of distance, because of the cube root), and w_1 and w_2 are weights (both set to 1.0 for this study).

Let the maximum expected storm speed be $s_{\max}$ (60 km h^{-1} was used). This is a constraint on the system, and may be incorporated by setting

C_{ij} equal to a large number if

$$d_p/\Delta t > s_{\max} \quad \text{(assumption 3)}. \tag{4}$$

This will ensure that the apparent cost of such a path is so high that it will not be included in the optimal set.

We wish to find the match that minimizes the objective function $Q = \sum C_{ij}$, where i refers to the start point of a path and j the corresponding end point, and the summation is performed over all possible sets of storm paths. The number of paths in the match will be less than or equal to the minimum of n_1 and n_2.

A problem posed in this manner can be transformed into a weighted matching or optimal assignment problem and can be solved using techniques from the field of combinatorial optimization. The transformed space has size $n \times n$, where n is the maximum of n_1 and n_2. The method has order $O(n^3)$. (The order of a method is a constant multiple of the maximum number of iterations required for solution.)

The optimal assignment problem can be stated in the following manner:

Given an $n \times n$ matrix $\mathbf{C}_{ij}$, find an $n \times n$ matrix $\mathbf{X}_{ij}$ such that the following hold:

1) In any given row or column, $\mathbf{X}_{ij}$ has exactly one nonzero element and that element has the value 1.

2) The sum of $\mathbf{C}_{ij}\mathbf{X}_{ij}$ over all i, j is a minimum.

We decided to use the Hungarian method for the solution since this method is relatively easy to implement and has order

$$O(p^2 q), \quad \text{where} \quad p = \min(n_1, n_2), \quad q = \max(n_1, n_2), \tag{5}$$

since in our case $\mathbf{C}_{ij}$ may have different numbers of rows and columns.

The Hungarian method algorithm first locates the largest set of zero elements in $\mathbf{C}_{ij}$, no two of which lie in the same row or column. If there are n such zero elements, then the positions of the $\mathbf{X}_{ij}$ can be set to match these zero elements in $\mathbf{C}_{ij}$, and the solution is complete. If not, the algorithm transforms the matrix $\mathbf{C}_{ij}$ by adding values to appropriate rows and columns to produce a new matrix $\mathbf{D}_{ij}$. It turns out that a solution to the optimal assignment problem for $\mathbf{D}_{ij}$ also solves the optimal assignment problem for $\mathbf{C}_{ij}$. If the matrix $\mathbf{D}_{ij}$ does not have the n zero elements in differing rows and columns, the algorithm will then continue to transform $\mathbf{D}_{ij}$. The algorithm guarantees that a solution will be found after a finite number of transformations.

The Hungarian method is both complicated and subtle. The short explanation given here is intended merely to introduce the reader to the method. Roberts (1984) gives a simple introduction to the method, and Lawler (1976) provides more detail, including information on the computer application of the method.

b. *Handling mergers and splits*

Quite frequently two or more convective storms will merge to form a single storm, and somewhat less frequently a single storm will split into two or more storms. This is particularly true of "storms" as they are defined in this paper. If the region between two storms exceeds the reflectivity threshold for a short time, the storms will appear to merge and then split soon thereafter.

The result of applying the matching scheme just described to mergers and splits is as follows:

- Merger—a maximum of one track will be extended, and the remainder will be terminated.
- Split—a maximum of one track will be extended,

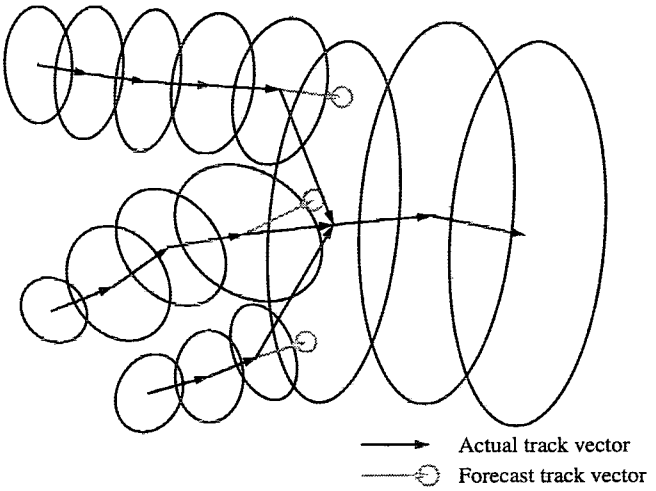

FIG. 4. Storm merger.

and new tracks will be created for the unmatched storms.

It is necessary to enhance the tracking scheme to handle these situations correctly. For example, consider Fig. 4, which shows the merger of three storms. The first step is to apply the matching algorithm as detailed above. Perhaps one track will be extended, and it may happen that none is extended. The latter occurs when the apparent movement of the centroid from the unmerged to merged situation is so great that the maximum speed constraint is violated. Then, we search through the storms at t_1 for those storms that were terminated at t_2 by the matching algorithm. For each of these tracks we are able to make a forecast of the centroid position at t_2 using the technique detailed in section 4. If this forecast position falls within the projected area of a storm at t_2, we conclude that the t_1 storm did not terminate but rather merged to form the t_2 storm.

The splitting situation is treated similarly (Fig. 5). In this case, for all the storms at t_1, we forecast the position, shape, and size of the projected-area ellipse at t_2. Then we consider all those storms at t_2 that are apparently new tracks, that is, have no history. If such a storm has a centroid located within the forecast projected-area ellipse of a storm, we conclude that a split has taken place.

4. Short-term forecasting

a. Methodology

In considering how to formulate the storm forecast algorithm, we make the following assumptions:

- A storm tends to move along a straight line.
- Storm growth or decay follows a linear trend.
- Random departures from the above behavior occur.

Forecasts are made for a number of parameters (listed in appendix D). The forecasts of importance to the tracking technique are reflectivity-weighted centroid, storm volume, and the parameters of the projected-area ellipse.

When a storm is observed for the first time, it has no history from which to make a forecast. In this case, all rates of change are assumed to be zero, and a persistence forecast is made. Forecasts at all later times are based on a linear trend model with double exponential smoothing (Abraham and Ledolter 1983). Simply stated, this is a linear regression model, in which the past values are weighted with exponentially decreasing weights.

Consider the time series p_i for a given storm parameter p, where ($i = 0$) is the present, ($i = 1$) is one time step in the past, and so on, and i ranges from 0 to $n_t - 1$, where n_t is the maximum number of time points considered relevant to the forecast. Let t_i be a measure of the time, for example, the number of seconds since the start of operations, and w_i be a weight associated with time step i.

For the exponentially smoothed model with parameter α, $w_i = \alpha^i$, where $0 < \alpha \leqslant 1$. A linear regression is performed between $w_i p_i$ and t_i. Figure 6 presents a simple example. The linear fit yields the equation of a straight line. The slope of the line is the forecast rate of change for the parameter p. It is assumed that the current value is correct, and the forecast is based on the current value and the forecast rate of change.

So if p_0 is the current value, and dp/dt is the estimated rate of change, then

$$p_t = p_0 + \left(\frac{dp}{dt}\right)\delta t. \tag{6}$$

For the forecast of the projected-area ellipse, it is assumed that the aspect ratio $r_{\text{major}}/r_{\text{minor}}$ and orientation θ remain constant. The forecast of the area A is based

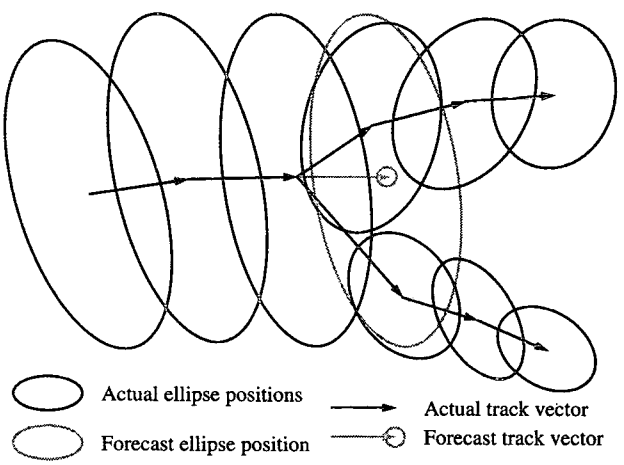

FIG. 5. Storm split.

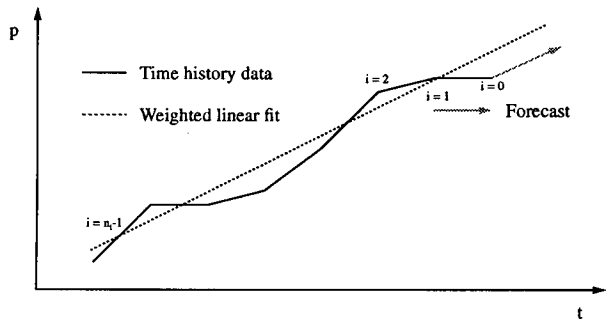

FIG. 6. Forecast based on weighted history.

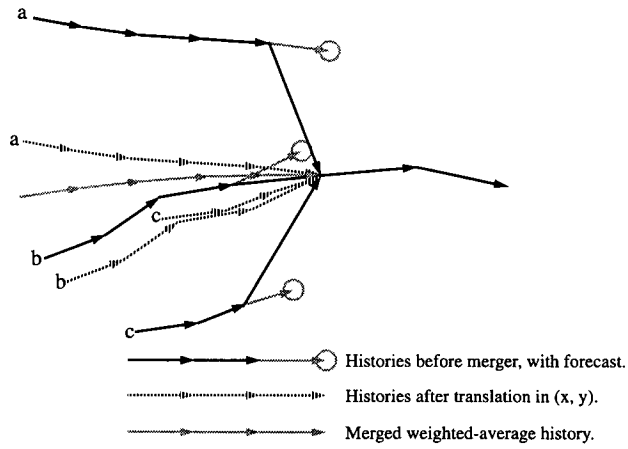

FIG. 7. Positional history translation for storm merger.

on the rate of change of volume rather than area, since the volume varies more smoothly with time than does the area, and therefore provides a less erratic forecast. So,

$$A_t = A_0 + \frac{A_0}{V_0}\left(\frac{dV}{dt}\right)\delta t. \tag{7}$$

For this study, the parameters used were $n_t = 6$ and $\alpha = 0.5$, and Δt was typically 6 min. For the type of storms studied, the forecast accuracy proved to be insensitive to α (Table 5).

b. *Handling mergers and splits*

The forecast depends on the recent storm history. Therefore, when a merger or split occurs, the history must be combined or split accordingly.

Let us first deal with the positional history. Consider the merger depicted in Fig. 4. The positional history of the merged track is a combination of the histories of the three parent tracks. First, the parent track histories are translated in (x, y) so that their forecast positions coincide with the centroid after the merger (Fig. 7). These translated histories are then combined as a weighted average, where the weights are the ratio of storm volume for each parent to the sum of the volumes of all parents. Clearly the weights change at each time in the history, depending on the size history of each of the parents. In the case of a split, the history of each child is a copy of the history of the parent, translated to coincide with the centroid of that child (Fig. 8).

Next consider the storm size parameters, such as area, volume, and mass. In the merger case, the history of a parameter is computed as the sum of the histories of the parents. In the split case, the history for a child is computed as the history for the parent scaled by the ratio of the volume of that child storm to the sum of the volumes of all of the children.

c. *Evaluation*

To evaluate the forecasts, both the forecast storm position (ellipse) and the "truth" (the actual radar echoes at the forecast time) are mapped onto a 5-km × 5-km grid. A grid point is considered "active" if any radar point in the area around that grid point exceeds the storm reflectivity threshold T_z.

The contingency table approach (Donaldson et al. 1975; Stanski et al. 1989) is used. The following definitions apply:

- Success—both truth and forecast grid points active.
- Failure—truth grid point active and forecast grid point inactive.
- False alarm—truth grid point inactive and forecast grid point active.

The probability of detection (POD), false-alarm ratio (FAR), and critical success index (CSI) are computed as follows:

$$\mathrm{POD} = \frac{n_{\mathrm{success}}}{n_{\mathrm{success}} + n_{\mathrm{failure}}}, \tag{8}$$

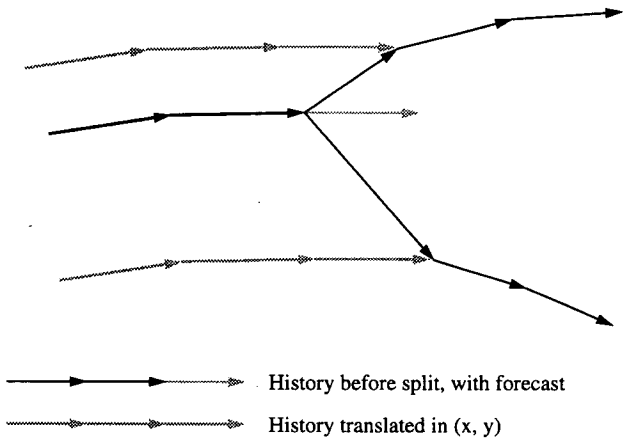

FIG. 8. Positional history translation for storm split.

$$\mathrm{FAR} = \frac{n_{\text{false alarm}}}{n_{\text{success}} + n_{\text{false alarm}}}, \quad (9)$$

$$\mathrm{CSI} = \frac{n_{\text{success}}}{n_{\text{success}} + n_{\text{failure}} + n_{\text{false alarm}}}. \quad (10)$$

The forecast results are presented in section 5.

5. Discussion and results

The data presented in this section are intended to show that the method works and to give the reader a feel for the type of results produced by the forecasting system. The analyses include data from all radar ranges (0–150 km), and no attempt was made to discriminate between storms in the mountains and those on the plains. A more detailed treatment of the results will be the subject of a later paper.

The system was run using real-time data from the Mile-High Radar near Denver for the summer of 1991, from 29 May to 29 August. Operations were generally limited to the hours from 1100 to 1900 MDT. The radar is a prototype similar to the WSR-88D (Pratte et al. 1991).

Figure 9 presents a typical plot of a storm track, showing the recent storm history, the present position, and the forecast.

A total of almost 4100 tracks were identified. Of these, 2000 were discarded for one or more of the following reasons:

- The storm existed at the beginning or end of radar operations, and therefore either the beginning or end of the track data were missing.
- The storm came too close to the radar for complete observation of the tops, or moved out of radar range (>150 km).
- The storm was observed during only one volume scan, resulting in a trivial track. This was the most common reason for rejection.

Of the 2100 or so "good" tracks remaining, 12% contained mergers or splits. Figure 10 presents the relationship between the duration and mean volume for each track, and indicates a positive correlation between duration and volume.

A few tracks in Fig. 10 have short durations and large mean volumes—these result from those cases in which the tracking algorithm fails to detect a merger or split and therefore discontinues the track for a mature storm and starts a new track for the same mature storm. If such a split follows a merger (or vice versa) the result may be a short track with a large mean volume. These failures occur for storms of very irregular shape because an ellipse does not fit the boundary well and the search for mergers and splits is confined to the interior of the ellipse. An improved algorithm that will

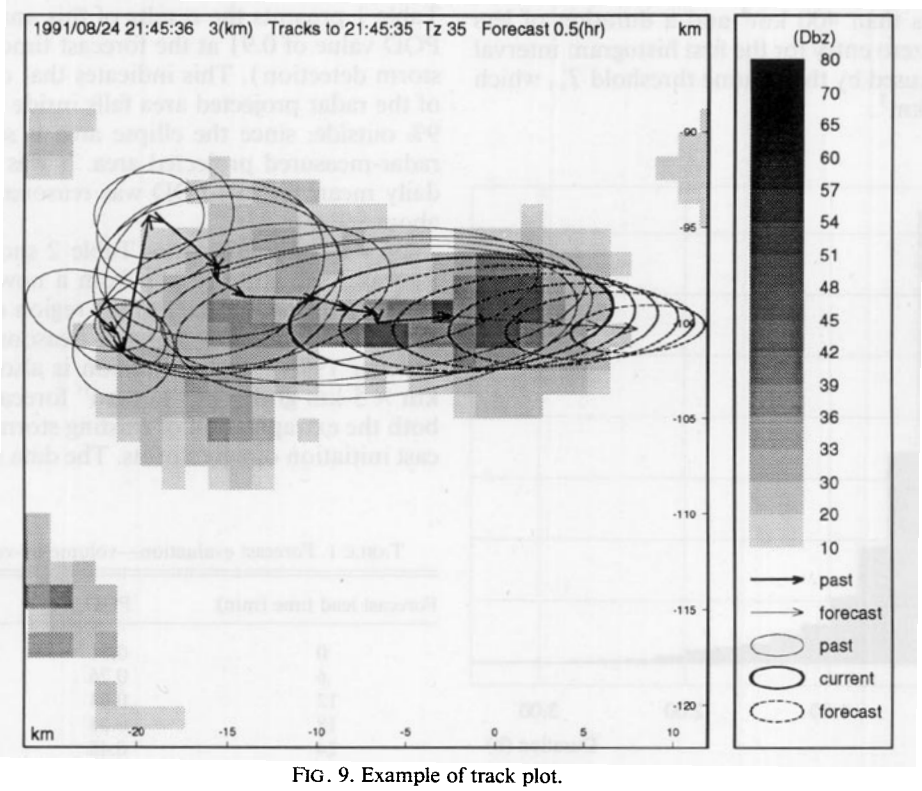

FIG. 9. Example of track plot.

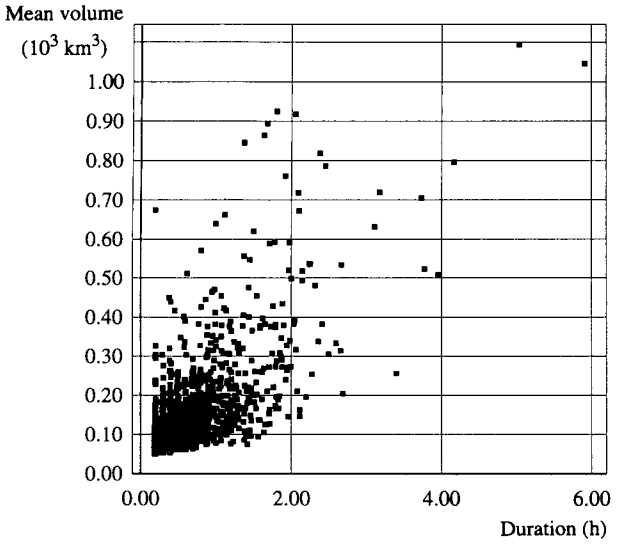

FIG. 10. Scatterplot of mean storm volume versus track duration.

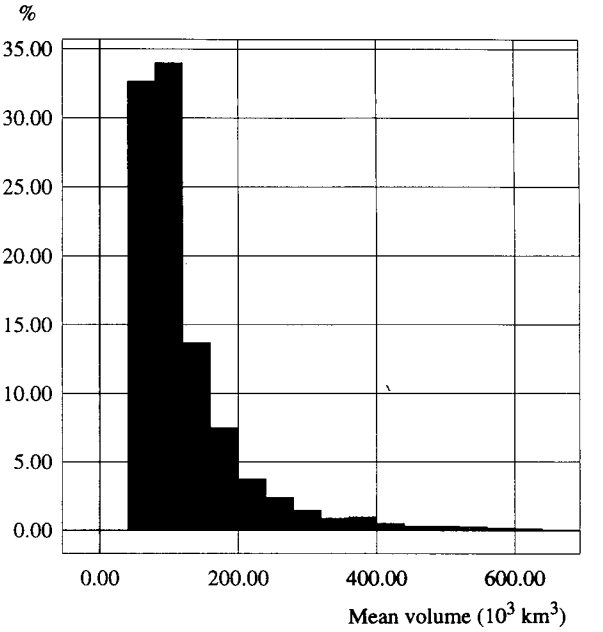

FIG. 12. Truncated histogram of mean storm volume per track.

describe the storm shape as a polygon rather than an ellipse is being tested, and indications are that this will do better for the identification of mergers of irregularly shaped storms.

Figures 11 and 12 show truncated histograms of the duration and mean volume of the storm tracks. The upper tails of the distributions, which have small values, have been truncated. From the figures it is clear that a large percentage of the storms are small, with a mean volume of less than 400 km^3 and a duration of less than 2 h. The zero entry for the first histogram interval in Fig. 12 is caused by the volume threshold T_v, which was set to 50 km^3.

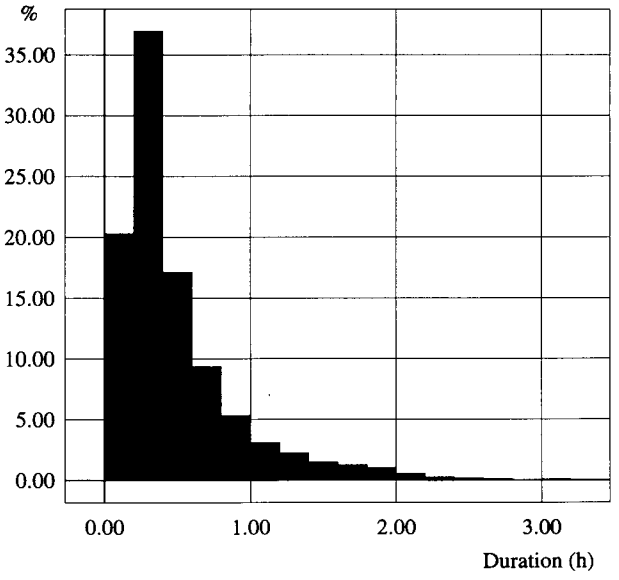

FIG. 11. Truncated histogram of storm-track duration.

The evaluation of the forecast accuracy was performed in a number of different ways, with minor variations between each. The simplest and most stringent approach is to consider the data on a volume-by-volume basis and compare the forecast positions of all of the storms with their actual positions as detected later. Table 1 presents the results of this analysis. Note the POD value of 0.91 at the forecast time of 0 min (i.e., storm detection). This indicates that on average 91% of the radar projected area falls inside the ellipse, and 9% outside, since the ellipse area is set equal to the radar-measured projected area. It was found that the daily mean for this POD was reasonably constant at about 90%.

By way of comparison, Table 2 shows the 30-min forecast evaluation results from a nowcasting experiment performed in the Denver region of Colorado for the 1989 and 1990 summer seasons (Wilson and Mueller 1993). The evaluation is also based on a 5-km × 5-km grid. The "human" forecasts incorporate both the extrapolation of existing storms and the forecast initiation of new storms. The data in Tables 1 and

TABLE 1. Forecast evaluation—volume-by-volume analysis.

Forecast lead time (min)	POD	FAR	CSI
0	0.91	0.13	0.80
6	0.76	0.28	0.59
12	0.64	0.40	0.45
18	0.55	0.48	0.36
24	0.48	0.56	0.30
30	0.42	0.62	0.25

TABLE 2. Forecast evaluation—Denver nowcasting experiment; forecast lead time 30 min.

Forecast type and date	POD	FAR	CSI
Human, 1989	0.62	0.68	0.27
Persistence, 1989	0.27	0.63	0.19
Human, 1990	0.55	0.85	0.14
Extrapolation only, 1990	0.15	0.75	0.10
Persistence, 1990	0.11	0.84	0.07

2 show that the accuracy of the automated forecasts is comparable with that of human forecasts. The following differences between the analyses should be noted:

- This method excludes all storms with a volume of less than 50 km^3, while the nowcasting experiment included all detectable storms.
- This method system used a 35-dBZ threshold for storm definition. The nowcasting experiment threshold was 30 dBZ for 1989 and 40 dBZ for 1990.
- This method only extrapolates existing storms, whereas the human forecasters attempted to handle initiation as well.

A problem with the preceding evaluation is that the analysis on a volume-by-volume basis includes all storms, even if they are too young for a forecast to be applicable to them. For example, if a storm is 15 min old, it is not possible for a 30-min forecast to have predicted its existence, since initiation is not dealt with. This complicates the evaluation by including cases for which the technique is not designed. If the aim is to analyze the method with a view to improvement, a more relevant approach is to perform the analysis on a track-by-track basis and include only those cases in which the storms are old enough to have been forecast, that is, for which the history exceeds the forecast lead time. Table 3 presents the results of the track-by-track analysis.

As a further condition on the analysis, one may evaluate only those cases in which the storms have sufficient history for one to reasonably expect the forecast to be accurate. The criterion used here is that the storm history must be at least half as long as the forecast lead time. Table 4 presents the results for this analysis.

Table 5 presents an analysis on the sensitivity of the forecast accuracy to the parameter α. Clearly, the accuracy is not very sensitive to the value of α, and the optimum lies between 0.25 and 0.75. An investigation was also carried out to determine the optimum value for n_t, the number of history volumes used in the forecast. An n_t value of 6 seems suitable for all values of α.

TABLE 3. Forecast evaluation—track-by-track analysis.

Forecast lead time (min)	POD	FAR	CSI
6	0.83	0.30	0.61
12	0.76	0.43	0.48
18	0.70	0.53	0.39
24	0.64	0.62	0.32
30	0.59	0.68	0.26

TABLE 4. Forecast evaluation—track-by-track analysis, with minimum required history.

Forecast lead time (min)	Minimum history (min)	POD	FAR	CSI
6	3	0.83	0.27	0.64
12	6	0.78	0.39	0.52
18	9	0.73	0.50	0.42
24	12	0.68	0.56	0.36
30	15	0.63	0.62	0.31

Tables 4 and 5 summarize the statistics for all of the tracks together. It is also useful to consider the forecast accuracy for individual tracks. We therefore analyzed each track, comparing the forecast storm locations with those observed for that track, and computed the POD, FAR, and CSI values averaged over the lifetime of the storm. Figures 13, 14, and 15 present scatterplots of POD, FAR, and CSI versus storm-track duration for a forecast lead time of 30 min and a minimum history of 15 min. Because of these constraints, the minimum duration for any track in the plots is 45 min. These plots show the range of forecast results that occur for storms of different durations. The scatter is large, indicating that the behavior of storms varies significantly and that the statistical forecasting model presented here performs much better in some cases than others.

6. Future enhancements

The method would benefit from the improvements discussed in this section.

a. Storm identification and tracking at multiple threshold levels

Some of the features that could be tracked using multiple threshold levels include

- individual cells within a convective storm,
- individual convective storms within a squall line,
- cellular features within a snow band.

TABLE 5. Sensitivity analysis for α—track-by-track analysis, with minimum required history, $n_t = 6$.

Forecast lead time (min)	Minimum history (min)	α	POD	FAR	CSI
30	15	0.26	0.617	0.620	0.307
30	15	0.50	0.630	0.620	0.310
30	15	0.75	0.628	0.630	0.303
30	15	1.00	0.625	0.641	0.298

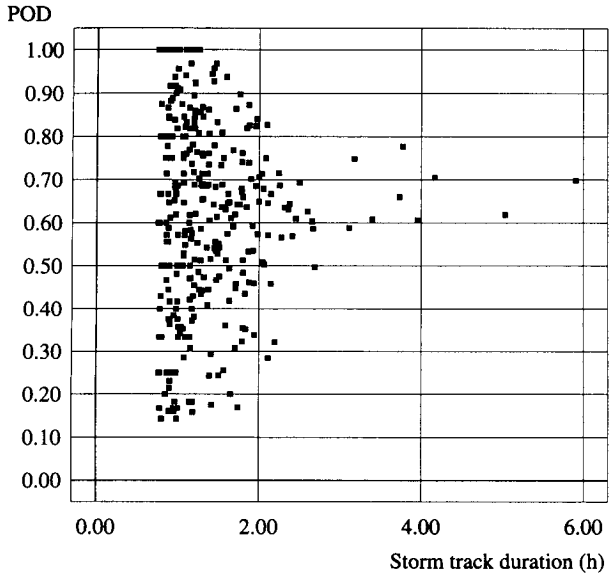

FIG. 13. Scatterplot of mean track POD versus storm-track duration; forecast lead time 30 min, minimum history 15 min.

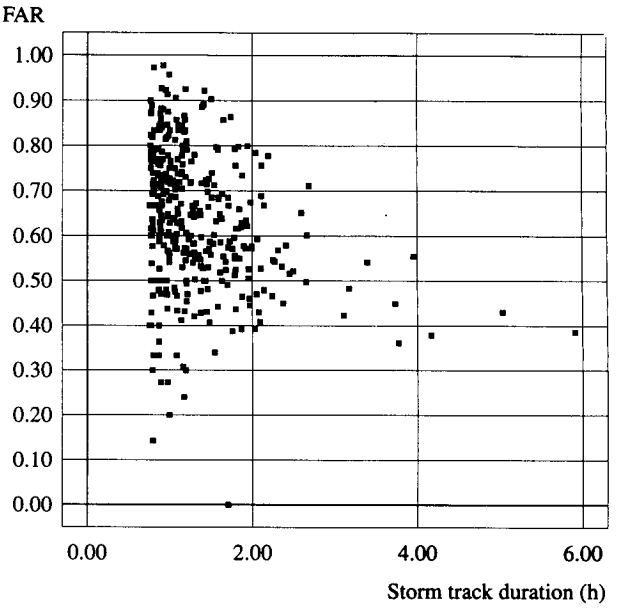

FIG. 14. Scatterplot of mean track FAR versus storm-track duration; forecast lead time 30 min, minimum history 15 min.

The identification of features using a higher reflectivity threshold, T_{z+}, is relatively simple once the identification at T_z is complete. The higher-intensity echo will be contained within the runs identified for the larger less-intense feature, and the search may be confined to those runs. Therefore the T_{z+} search does not add significantly to the computations.

b. Incorporation of a more detailed shape representation for the projected area

The possibility of using shapes other than ellipses to depict the projected area is currently under investigation. The ellipse was chosen as the initial candidate because of its simplicity. Other potential shape categories include

- arbitrary curvilinear shapes,
- convex polygons,
- arbitrary polygons.

c. Using additional storm properties to sharpen the forecast

The storms and their tracks have well-defined properties. It seems probable that some of these contain information that could be used to amend the forecast. For example, a multivariate correlation analysis between storm volume and other properties, the volume being lagged in time, could yield a lagged linear model for volume forecasts.

7. Hardware requirements

This system is data driven in that it needs to keep pace with a real-time radar data stream. It was found that all of the processing required, including display, can be adequately performed on two workstations in the 10–15-MIPS (million instructions per second) class, and from initial tests it appears that a single workstation in the 20-MIPS class would be able to perform all of the functions.

8. Conclusions

This methodology provides the framework necessary to identify storms within three-dimensional radar data

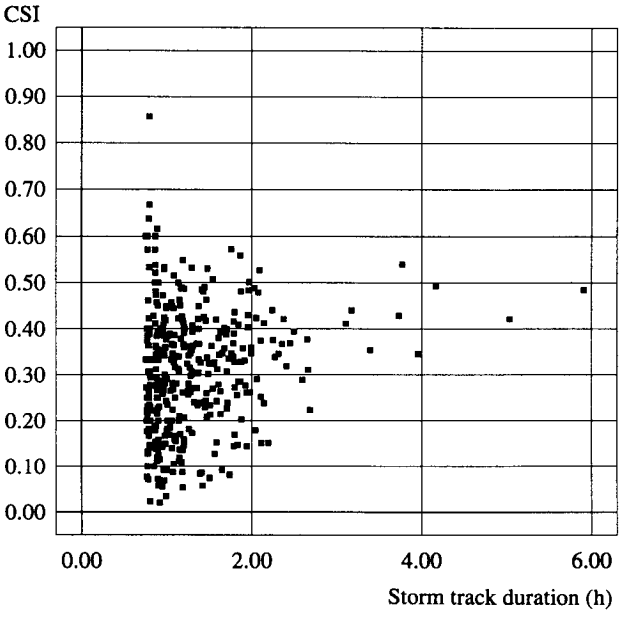

FIG. 15. Scatterplot of mean track CSI vs storm-track duration; forecast lead time 30 min, minimum history 15 min.

and to track them as physical entities. The storm and track data are suitable for scientific analysis, for the purposes of both understanding and forecasting the physics of storm development and movement.

The method was successfully applied during real-time operations for a summer season in Colorado, and the human observers felt that typically it performed well. The accuracy of the forecasts is encouraging and is comparable with that of human-based forecasts that take additional factors such as low-level convergence and storm initiation into account. The intention is to use the system to assist forecasters in future field projects, who will in turn provide feedback on how well the system performs, and what enhancements should be made.

APPENDIX A

Cartesian Transformation and Noise Filtering

The Cartesian transformation is performed using the "nearest neighbor" principle with no interpolation. It is assumed that the radar will be operated using a fixed scan strategy. For each point in the target Cartesian grid, the coordinates of the closest radar point are computed and stored in a table. This table is then inverted, so that the target Cartesian locations for each radar point are known. When a radar beam is processed, the gate data are placed directly into the appropriate place in the Cartesian grid. Typically, there are radar points to which multiple Cartesian points correspond (long ranges, radar undersampling) and radar points with no corresponding Cartesian point (short ranges, radar oversampling).

During the transformation, noise suppression is carried out. A signal-to-noise threshold T_{sn} (dBm), is set. Any radar point with a signal-to-noise value below T_{sn} is considered to contain missing data. This removes much of the noise, but leaves some "spotty" areas where the noise spikes exceed T_{sn}. Such spikes could be caused by receiver noise, or point targets such as birds, aircraft, and ground targets. Removal of these spots is accomplished in a second step. Let $L_{\min}$ be the minimum dimension for any feature considered valid. The data from each beam are searched for runs of data above T_{sn} but with a length less than $L_{\min}$. Such runs are flagged as missing data. For this study, T_{sn} was set to 10.0 dB, and $L_{\min}$ to 1.2 km.

APPENDIX B

Clutter Removal

Ground clutter presents a problem if the size of a region of clutter exceeds $V_{\min}$. In the case of the Mile-High Radar near Denver, which provided the data for this study, the Rocky Mountains cause significant clutter regions.

The clutter map is computed from a number of Cartesian volumes (at least 20) sampled during a period of no significant weather. The signal-to-noise ratio $T_{sn\_clutter}$ applied to these volumes is set somewhat lower than T_{sn}. The reason for this is to include clutter points that are borderline, and that may exceed T_{sn} only some of the time. The clutter value for a Cartesian grid point is computed as the median of the reflectivity values at that grid point for all of the clear-air scans.

This clutter map is then used to filter out clutter during the Cartesian transformation stage. A grid point is considered to contain clutter if the reflectivity does not exceed the clutter map value plus some clutter margin.

The relevant values used for this study were $T_{sn\_clutter}$ = 4.0 dB with a clutter margin of 6.0 dB.

This clutter removal methodology is based on Hynek (1990), and this reference should be consulted for further details.

APPENDIX C

Computed Storm Parameters

The following storm parameters were computed:

- centroid for whole storm and for each plane,
- reflectivity-weighted centroid for whole storm and for each plane,
- top,
- base,
- volume,
- area for each plane, and mean area,
- mass of precipitation for whole storm and for each plane (based on Z–M relationship),
- rain flux (based on Z–R relationship),
- angle and direction of tilt,
- max and mean reflectivity for whole storm and for each plane,
- height of max reflectivity,
- estimate of vorticity about a vertical axis through the storm centroid (based on circular storm model) for whole storm and for each plane,
- mean and standard deviation of velocity for whole storm and for each plane,
- mean and standard deviation of spectral width for whole storm and for each plane,
- position, size, and shape of rain region (lowest plane),
- position, size, and shape of projected area,
- histogram of reflectivity as function of volume,
- histogram of reflectivity as function of area.

APPENDIX D

Forecast Parameters

The following forecast parameters were computed:

- centroid,
- reflectivity-weighted centroid,
- top,
- base,
- volume,

- mean area,
- mass of precipitation (based on Z–M relationship),
- rain flux (based on Z–R relationship),
- rain area,
- projected area.

APPENDIX E

Computation of Rotated Ellipse Parameters

The parameters of the rotated ellipse fitted to the projected area are derived from the parameters of a principal component transformation applied to the (x, y) data pairs that make up the projected area.

Refer again to Fig. 2. Suppose there are n (x, y) pairs, each of which represent a grid point in the projected area of the storm. Then

$$\bar{x} = \frac{1}{n}\sum_{i=1}^{n} x_i, \quad \bar{y} = \frac{1}{n}\sum_{i=1}^{n} y_i. \tag{E1}$$

An estimate of the covariance matrix of the (x, y) data is given by

$$\mathrm{cov}_{xy} = \begin{bmatrix} d & e \\ e & f \end{bmatrix}, \quad \text{where} \tag{E2}$$

$$d = \frac{1}{n-1}\sum_{i=1}^{n} (x_i - \bar{x})^2, \tag{E3}$$

$$e = \frac{1}{n-1}\sum_{i=1}^{n} (x_i - \bar{x})(y_i - \bar{y}), \tag{E4}$$

$$f = \frac{1}{n-1}\sum_{i=1}^{n} (y_i - \bar{y})^2. \tag{E5}$$

The principal component transformation is based on an eigenvalue–eigenvector analysis of the covariance matrix. For computer implementations, the best approach is to use a general purpose numerical eigenvector solver because these take care of all of the special cases that may arise, and that are data dependent. However, for completeness, we will include the equations that describe the two-dimensional analysis as it is applied to the ellipse problem.

The eigenvalues of the covariance matrix are given by

$$\lambda_1, \lambda_2 = \frac{(d+f) \pm [(d+f)^2 - 4(df - e^2)]^{1/2}}{2}, \tag{E6}$$

where λ_1 is the larger of the two eigenvalues. Here λ_1 represents the variance of the data in the u direction, and λ_2 the variance in the v direction. Therefore,

$$\sigma_{\mathrm{major}} = \lambda_1^{1/2}, \quad \sigma_{\mathrm{minor}} = \lambda_2^{1/2}, \tag{E7}$$

where σ_{major} and σ_{minor} are the standard deviation of the data in the u and v directions, respectively.

The normalized (μ, ν) eigenvector in (u, v) coordinates associated with λ_1 is given by

$$\nu = \left[\frac{1}{(1+g^2)}\right]^{1/2}, \quad \mu = -g\nu, \quad \text{where} \tag{E8}$$

$$g = \frac{f + e - \lambda_1}{d + e - \lambda_1}. \tag{E9}$$

The ellipse properties are computed as follows. The centroid position is given by the mean of the (x, y) data

$$(\bar{x}_e, \bar{y}_e) = (\bar{x}, \bar{y}). \tag{E10}$$

The rotation θ of the ellipse major axis relative to the x axis is given by

$$\theta = \tan^{-1}\left(\frac{\nu}{\mu}\right). \tag{E11}$$

The area of the storm, A, is given by

$$A = ndxdy, \tag{E12}$$

where dx and dy are the Cartesian grid spacing in x and y, respectively.

We set the ellipse area to be equal to the storm area. The major and minor radii of the ellipse are therefore given by

$$r_{\mathrm{minor}} = \sigma_{\mathrm{minor}}\left(\frac{A}{\pi\sigma_{\mathrm{major}}\sigma_{\mathrm{minor}}}\right)^{1/2},$$

$$r_{\mathrm{major}} = \sigma_{\mathrm{major}}\left(\frac{A}{\pi\sigma_{\mathrm{major}}\sigma_{\mathrm{minor}}}\right)^{1/2}. \tag{E13}$$

REFERENCES

Abraham, B., J. Ledolter, 1983: *Statistical Methods for Forecasting.* Wiley, 445 pp.

Austin, G. L., 1985: Application of pattern-recognition and extrapolation techniques to forecasting. *Eur. Space Agency J.*, **9**, 147–155.

——, and A. Bellon, 1982: Very-short-range forecasting of precipitation by the objective extrapolation of radar and satellite data. *Nowcasting,* A. K. Browning, Ed., Academic Press, 177–190.

Crane, R. K., 1979: Automatic cell detection and tracking. *IEEE Trans. Geosci. Electron.*, **GE-17,** 250–262.

Dixon, M. J., and G. K. Mather, 1986: Radar evaluation of a randomized rain-augmentation experiment—Some preliminary results. Preprints, *10th Conf. on Planned and Inadvertent Weather Modification,* Arlington, Virginia, Amer. Meteor. Soc., 139–141.

Donaldson, R. J., R. M. Dyer, and M. J. Kraus, 1975: An objective evaluation of techniques for predicting severe weather events. Preprints, *9th Conf. on Severe Local Storms,* Norman, Oklahoma, Amer. Meteor. Soc., 321–326.

Hynek, D. P., 1990: Use of clutter residue editing maps during the Denver 1988 Terminal Doppler Weather Radar (TDWR) tests. Project Rep. ATC-169, MIT Lincoln Laboratory, Lexington, MA, 65 pp.

Lawler, E. L., 1976: *Combinatorial Optimization: Networks and Matroids.* Holt, Rinehart and Winston, 201–207.

Pratte, J. F., J. H. Van Andel, D. G. Ferraro, R. W. Gagnon, S. M. Maher, G. L. Blair, 1991: NCAR's mile high meteorological

radar. Preprints, *25th Int. Conf. on Radar Meteorology,* Paris, France, Amer. Meteor. Soc., 863–866.

Richards, J. A., 1986: *Remote Sensing Digital Image Analysis—An Introduction.* Springer-Verlag, 127–142.

Rinehart, R. E., and E. T. Garvey, 1978: Three-dimensional storm motion detection by conventional weather radar. *Nature,* **273,** 287–289.

Roberts, F. S., 1984: *Applied Combinatorics.* Prentice-Hall Inc., 565–568.

Rosenfeld, D., 1987: Objective method for analysis and tracking of convective cells as seen by radar. *J. Atmos. Oceanic Technol.,* **4,** 422–434.

Stanski, H. R., L. J. Wilson, and W. R. Burrows, 1989: Survey of common verification methods in meteorology. World Weather Watch Tech. Rep. No. 8, World Meteorological Organization, Geneva, Switzerland, 114 pp.

Tuttle, J. D., and G. B. Foote, 1990: Determination of the boundary layer airflow from a single Doppler radar. *J. Atmos. Oceanic Technol.,* **7,** 218–232.

Wilson, J. W., and W. E. Schreiber, 1986: Initiation of convective storms at radar-observed boundary-layer convergence lines. *Mon. Wea. Rev.,* **114,** 2516–2536.

——, and C. K. Mueller, 1993: Nowcasts of thunderstorm initiation and evolution. *Wea. Forecast.,* **8,** 113–131.

Witt, A., and J. T. Johnson, 1993: An enhanced storm cell identification and tracking algorithm. Preprints, *26th Int. Conf. on Radar Meteorology,* Norman, Oklahoma, Amer. Meteor. Soc., in press.

Zittel, W. D., 1976: Computer applications and techniques for storm tracking and warning. Preprints, *17th Int. Conf. on Radar Meteorology,* Seattle, Amer. Meteor. Soc., 514–521.